Analytical Methods

PAPER

View Article Online
View Journal | View Issue

Cite this: *Anal. Methods*, 2019, **11**, 2396

A turn-on near-infrared fluorescent probe with rapid response and large Stokes shift for the selective and sensitive detection of zinc(II) and its application in living cells†

Weixia Zhang, Xinxin Jin, Wei Chen, Chunhui Jiang* and Hongfei Lu *

Received 22nd February 2019
Accepted 2nd April 2019

DOI: 10.1039/c9ay00380k

rsc.li/methods

Herein, a new near-infrared turn-on fluorescent probe, **YPT**, was designed and synthesized for the rapid detection of Zn^{2+}, which exhibited low limit of detection for Zn^{2+} (12 nM) as well as a favorable large Stokes shift ($\lambda_{em} - \lambda_{ex} = 168$ nm). In addition, the probe showed rapid detection progress within 30 s, accompanied by a distinct change in fluorescence from colorless to bright red. Moreover, the sensing mechanism of **YPT** towards Zn^{2+} was supported by the Job's plot, HR-MS analysis, ^{1}H NMR titration analysis and density functional theory (DFT) results. In addition, **YPT** was applied as a visible test strip for the detection of Zn^{2+}. Finally, the NIR fluorescence imaging of Zn^{2+} was successfully performed in living cells using this probe. All the results indicate that this probe can be used to detect Zn^{2+} in both solution and living systems.

1 Introduction

Zinc is considered as the second most abundant transition metal element after iron in the human body and has significant influence on various biological processes including gene expression, neural signal transmission and DNA binding or recognition.[1–6] Moreover, zinc mainly acts as a structural and catalytic cofactor in proteins.[7] Thus, an appropriate amount of zinc is beneficial for human health. On the other hand, zinc deficiency can lead to some serious diseases such as low blood sugar, Alzheimer's disease, Parkinson's disease, epilepsy and cerebral ischemia.[8–11] Therefore, it is of great importance to develop sensitive and selective tools for the detection of zinc to monitor human health.

A number of traditional analytical methods, mainly including atomic absorption spectrometry (AAS), atomic emission spectrometry (AES), inductively coupled plasma mass spectrometry with microprobes and electrochemical methods, have been established for the detection of zinc;[12–16] however, all these approaches need sophisticated and expensive instruments, rigorous experimental conditions, as well as long time for detection. Compared with these methods, fluorescent probes have been paid significant attention owing to their excellent selectivity, high sensitivity, shorter detection time, operational simplicity and low cost towards zinc monitoring.[17–19]

To date, some fluorescent zinc probes have been developed. These probes were mainly derived from fluorescein,[20] tetraphenylethene,[21] anthryl,[22] BODIPY,[23,24] coumarin,[25] triphenylethylene,[26–28] and fluorescent pyrene derivatives.[29,30] Despite the achievement of these probes, the development of probes for zinc still remains a challenging task because of their intrinsic properties such as narrow Stokes shift (<60 nm), long response time (typically >20 min) and fluorescence changes in a short wavelength window (<600 nm).[31–34] To overcome these limitations, red-NIR fluorescent probes are applicable alternatives owing to their minimal background interference, improved tissue depth penetration and high image sensitivities.[35–37] Thus, there is still a strong demand for the design of red-NIR fluorescent probes towards the detection of zinc.

In this regard, dicyanoisophorone-based dyes have certain excellent advantages including large Stokes shift, emissions in the NIR region, good photostability and less toxicity.[38,39] Therefore, dicyanoisophorone-based dyes have been widely used in dye-sensitized solar cells, organic nonlinear optical crystals and fluorescent dyes.[40,41] Purine derivatives are well used in the construction of biological probes due to their low toxicity.[42] Moreover, the purine derivatives that bear a heteroatom have good binding ability.[43,44] On this basis, we developed a new dicyanoisophorone-based fluorescent **YPT** from a purine derivative moiety with the remarkable nature of a naked-eye 'off–on' sensing system for the detection of zinc (Scheme 1). Importantly, this probe exhibited excellent sensitivity and selectivity (detection limit: 12 nM) and rapid response (within

School of Biology and Chemical Engineering, Jiangsu University of Science and Technology, 212003 Zhenjiang, China. E-mail: zjluhf1979@just.edu.cn; chemjiang@just.edu.cn

† Electronic supplementary information (ESI) available. See DOI: 10.1039/c9ay00380k

30 s). Furthermore, **YPT** was successfully used for the bio-imaging of Zn^{2+} in living cells and applied as a visible test strip for the detection of Zn^{2+} in water.

2 Experimental

2.1 Materials and methods

All chemicals were purchased from Energy Chemical, and all solvents were obtained from Shanghai Wohua Chemical Wohua Co. Ltd. All reagents and organic solvents were used as received without further purification, and double distilled water was used throughout the experiments. Thin layer chromatography (TLC) analysis was conducted using the Haiyang silica gel F254 plate, and column chromatography was conducted using Haiyang silica gel (mesh: 200–300, 300–400).

2.2 General instrumentation

The ^{1}H NMR and ^{13}C NMR spectra were obtained *via* the Bruker-Avance DPX 400 MHz spectrometer using DMSO-d_6 as a solvent and tetramethylsilane (TMS, 0.00 ppm) as an internal standard. Mass spectrometry was performed using Agilent-6110. Elemental analysis was performed by Germany Elementar Vario EL. Melting points were determined by the XY-51 melting point apparatus. High-resolution mass spectrometry (HRMS) spectra were obtained using the Bruker microTOF-Q instrument. Fluorescence spectra were obtained using the spectrofluorometer FS5. UV-vis absorption spectra were acquired using the U3010-vis spectrophotometer. The pH levels were detected using FE20. The cell viability assay was carried out by CCK-8. Cell images were obtained using a laser confocal microscope (Leica TCS SP2 AOBS).

2.3 Synthesis

2.3.1 Synthesis of compound 1. To a solution of malononitrile (1.87 g, 28.3 mmol) and isophorone (3.9 g, 28.3 mmol) in DMF (10 mL), two drops of piperidine, two drops of acetic acid, and ten drops of acetic anhydride were added. The mixture was stirred for 1 h and then heated at 80 °C for 1 h. After this, 4-hydroxybenzaldehyde (3.45 g, 28.7 mmol) was added to the abovementioned mixture under a N_2 atmosphere for 1 h, and the mixture was then poured into 200 mL water containing 6 mL of concentrated hydrochloric acid. The precipitate was obtained by filtration and recrystallized by acetonitrile to afford the compound **1** as a red solid (3.53 g, 43%).

^{1}H NMR (400 MHz, DMSO-d_6) δ: 9.99 (s, 1H), 7.63–7.49 (m, 2H), 7.30–7.13 (m, 2H), 6.85–6.75 (m, 3H), 2.59 (s, 2H), 2.53 (s, 2H), 1.01 (s, 6H). ^{13}C NMR (101 MHz, DMSO-d_6) δ: 170.72, 159.79, 157.15, 138.74, 130.32, 127.58, 126.70, 121.83, 116.35, 114.58, 113.77, 75.28, 42.80, 38.67, 32.12, 27.90. ESI-MS: calcd for $[M–H]^+$ 289.14, found 289.1.

2.3.2 Synthesis of compound 2. A solution of compound **1** (580 mg, 2 mmol) in 10 mL trifluoroacetic acid was added to hexamethylenetetramine (272 mg, 1.94 mmol). After being refluxed for 2 h, the reaction mixture was cooled down to room temperature and poured into ice water. The precipitate was obtained by filtration and further purified by silica gel chromatography to produce a yellow powder (312 mg, 49%).

^{1}H NMR (400 MHz, DMSO-d_6) δ: 11.18 (s, 1H), 10.28 (s, 1H), 7.96 (d, J = 2.3 Hz, 1H), 7.88 (dd, J = 8.7, 2.4 Hz, 1H), 7.29 (d, J = 1.5 Hz, 2H), 7.04 (d, J = 8.7 Hz, 1H), 6.85 (d, J = 1.2 Hz, 1H), 2.59 (s, 2H), 2.52 (s, 1H), 1.01 (s, 6H). ^{13}C NMR (101 MHz, DMSO-d_6) δ: 191.14, 170.71, 162.25, 156.53, 137.15, 135.58, 129.26, 76.26, 42.75, 38.61, 32.10, 27.90.

2.3.3 Synthesis of compound 3. To a mixture of 5-amino-4,6-dichloropyrimidine (2.5 g, 15 mmol) and 1-naphthylamine (4.292 g, 30 mmol) in methanol (25 mL), HCl (2.5 mL, 30 mmol) was added followed by refluxing for 24 h. The mixture was cooled down to room temperature and evaporated under reduced pressure. The residue was dissolved in 1 N NaOH, and the solution was extracted with ethyl acetate (3 × 40 mL) followed by the removal of solvents under reduced pressure. The crude product was purified by recrystallization using methanol–H_2O (1 : 5). The compound **3** was obtained as a pale violet powder (2.795 g, 69%)

^{1}H NMR (400 MHz, DMSO-d_6) δ: 8.79 (s, 1H), 8.00–7.94 (m, 1H), 7.89 (ddd, J = 7.4, 2.2, 0.9 Hz, 1H), 7.86–7.81 (m, 1H), 7.64 (s, 1H), 7.56 (d, J = 2.2 Hz, 1H), 7.54 (d, J = 2.6 Hz, 1H), 7.53 (t, J = 2.3 Hz, 1H), 5.76 (s, 1H), 5.47 (s, 2H). ESI-MS: calcd for $[M + H]^+$ 271.07, found 271.1. Mp 173.8–175. 1 °C.

2.3.4 Synthesis of compound 4. A solution of compound **3** (1.968 g, 7.3 mmol), PPA (9.868 g, 29.2 mmol), acetic acid (2.19 g, 36.5 mmol) and DTAC (0.193 g, 10% mmol) in $POCl_3$ (20 mL) was stirred at 80 °C overnight. After the starting materials disappeared, the mixture was cooled down to room temperature and evaporated under reduced pressure. Then, ice water was poured to the mixture, which was then filtered to obtain a light yellow powder (1.03 g, 48%).

^{1}H NMR (400 MHz, DMSO-d_6) δ: 8.60 (s, 1H), 8.26 (dt, J = 8.0, 1.1 Hz, 1H), 8.17 (d, J = 8.2 Hz, 1H), 7.83–7.73 (m, 2H), 7.66 (ddd, J = 8.2, 6.9, 1.2 Hz, 1H), 7.52 (ddd, J = 8.3, 6.9, 1.3 Hz, 1H), 7.21 (dd, J = 8.5, 1.0 Hz, 1H), 2.38 (s, 3H). ^{13}C NMR (101 MHz, DMSO-d_6) δ: 156.89, 151.31, 148.73, 145.94, 134.27, 130.78, 130.51, 130.10, 128.93, 128.38, 127.41, 127.19, 126.20, 123.55, 122.33, 14.11. ESI-MS: calcd for $[M + H]^+$ 295.07, found 295.1.

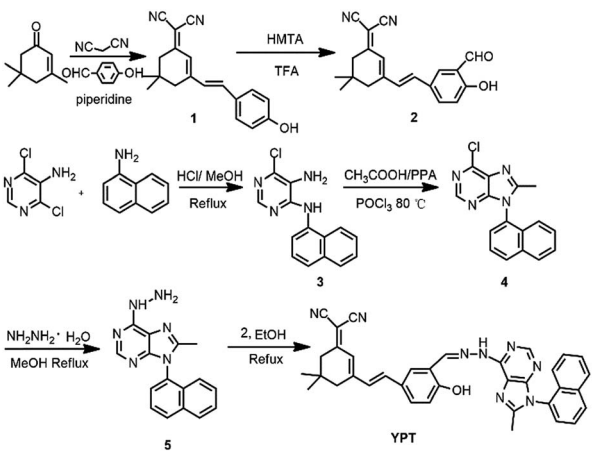

Scheme 1 The synthetic route of **YPT**.

Mp 223.6–224.7 °C. Elemental analysis (%): calcd C 65.20, N 19.01, H 3.76; found, C 65.31, N 19.15, H 3.77.

2.3.5 Synthesis of compound 5. Compound **4** (1.371 g, 4.67 mmol) was dissolved in methanol (30 mL), and then, hydrazine was added to the mixture followed by refluxing for 3 h. The reaction mixture was cooled down to room temperature and filtered to obtain a light yellow powder (1.219 g, 90%).

^{1}H NMR (400 MHz, DMSO-d$_6$) δ: 9.00 (s, 1H), 8.20 (dt, J = 7.9, 1.2 Hz, 1H), 8.13 (dd, J = 8.2, 1.1 Hz, 1H), 8.07 (s, 1H), 7.75–7.68 (m, 2H), 7.63 (ddd, J = 8.2, 6.9, 1.2 Hz, 1H), 7.51 (ddd, J = 8.3, 6.9, 1.3 Hz, 1H), 7.05 (dd, J = 8.4, 1.1 Hz, 1H), 4.61 (s, 2H), 2.24 (s, 3H). ^{13}C NMR (101 MHz, DMSO-d$_6$) δ: 156.86, 155.05, 151.87, 148.05, 134.34, 131.03, 130.02, 129.81, 129.02, 127.56, 122.34, 14.74. ESI-MS: calcd for $[M + H]^+$ 291.13, found 291.1. Mp 224.6–225.9 °C. Elemental analysis (%): calcd C 66.19, N 28.95, H 4.86; found, C 66.21, N 29.05, H 4.74.

2.3.6 Synthesis of compound YPT. Compound **2** (1.75 g, 5.5 mmol) and compound **5** (1.451 g, 5 mmol) were dissolved in ethanol (60 mL), and the mixture was refluxed for 5 h. Then, the mixture was filtered and washed three times with ethanol. The compound **YPT** was obtained as a red solid (2.542 g, 85%).

^{1}H NMR (400 MHz, DMSO-d$_6$) δ: 12.15 (s, 1H), 11.93 (s, 1H), 8.34 (s, 1H), 8.26–8.19 (m, 2H), 8.17–8.13 (m, 1H), 7.80–7.72 (m, 3H), 7.68–7.58 (m, 2H), 7.53 (ddd, J = 8.3, 6.9, 1.3 Hz, 1H), 7.26 (d, J = 2.3 Hz, 2H), 7.13 (dd, J = 8.5, 1.1 Hz, 1H), 6.99 (d, J = 8.5 Hz, 1H), 6.81 (s, 1H), 2.60 (s, 2H), 2.54 (d, J = 6.5 Hz, 2H), 2.31 (s, 3H), 1.02 (s, 6H). ^{13}C NMR (101 MHz, DMSO-d$_6$) δ: 170.62, 158.75, 156.76, 152.38, 151.41, 144.63, 137.81, 134.35, 130.80, 130.54, 130.11, 128.97, 128.32, 127.91, 127.54, 127.42, 127.32, 126.26, 122.44, 122.22, 119.79, 118.18, 114.45, 113.69, 75.68, 42.76, 38.65, 32.09, 27.93, 14.52. ESI-MS: calcd for $[M–H]^+$ 589.25, found 589.2. Elemental analysis (%): calcd C 73.20, N 18.97, O 2.71, H 5.12; found, C 73.25, N 18.95, O 2.72, H 5.08.

2.4 General procedure for UV-vis and fluorescence spectroscopy experiments

The stock solutions (1 mM) of metal salts (*i.e.* Zn^{2+}, Ag^+, Ni^{2+}, Cs^{2+}, Fe^{3+}, Hg^{2+}, Ca^{2+}, Mg^{2+}, Co^{2+}, K^+, Cu^{2+}, Na^+, Al^{3+}, Pt^{2+}, Cd^{2+}, Pb^{2+}, Cr^{3+}, Ba^{2+} and Pd^{2+}) were prepared in DMSO–H_2O (3 : 2 v/v, pH 7.4, HEPES buffer, 0.5 mM). The stock solution of the probe **YPT** (1 mM) was prepared in DMSO–H_2O (3 : 2 v/v, pH 7.4, HEPES buffer, 0.5 mM). The UV-vis spectra and fluorescence spectra were obtained at room temperature (λ_{ex} = 502 nm, λ_{em} = 670 nm slit: 2.5 nm/2.5 nm). Statistical analysis of the data was carried out by Origin 8.

2.5 Preparation of paper test strips

Filter papers were dipped in the stock solution of **YPT** (1 mM), and then, the test strips coated with **YPT** were dried in air to measure different concentrations of Zn^{2+}.

2.6 Cell studies of YPT

2.6.1 Cytotoxicity of YPT. **YPT** was dissolved in DMSO to prepare a stock solution. Then, HeLa cells were incubated with **YPT** at concentrations ranging from 0 to20 μM. Lastly, MTT assays for HeLa cells were performed to determine the cytotoxicity of **YPT**.

2.6.2 Fluorescence imaging in living cells. In the control group, the HeLa cells were incubated with 10 μM of **YPT** at 37 °C. After 30 min, the cells were washed three times with PBS buffer and then imaged. In the experimental group, the HeLa cells were treated with **YPT** (10 μM) for 30 min at 37 °C, washed three times with PBS, and then treated with 20 μM of Zn^{2+}. After this, the HeLa cells were imaged using a confocal microscope.

3 Results and discussion

3.1 UV-vis absorption and fluorescence spectral studies

After the probe was obtained, we first determined the feasibility of Zn^{2+} sensing by **YPT** using the UV-vis absorption and fluorescence spectra obtained in DMSO–H_2O (3 : 2 v/v, pH 7.4, HEPES buffer, 0.5 mM). As shown in Fig. 1, the?> UV-vis spectra of free **YPT** (10 μM) exhibited an absorption peak with maximum at 434 nm; however, upon the addition of 5.0 equiv. of Zn^{2+} to this solution, the maximum absorption peak red-shifted to 502 nm. Compared with that of **YPT**, the spectrum of **YPT** + Zn^{2+} exhibits a red shift of 68 nm. Moreover, **YPT** displayed weak fluorescence emission upon the addition of 5.0 equiv. of Zn^{2+}, and the fluorescence intensity of the reaction solution reached the maximum value at 670 nm. Moreover, we found that the large Stokes shift ($\lambda_{em} - \lambda_{ex}$) of the probe **YPT** could reach up to 168 nm, which was highly beneficial because it effectively reduced the background interference caused by the excitation and scattered light in practical applications.

3.2 Selectivity of YPT towards various analytes

High selectivity is one of the most significant properties for a fluorescent probe. To evaluate the selectivity of the proposed probe, various common and important metal ions, such as Zn^{2+}, Ag^+, Ni^{2+}, Cs^{2+}, Fe^{3+}, Hg^{2+}, Ca^{2+}, Mg^{2+}, Co^{2+}, K^+, Cu^{2+}, Na^+, Al^{3+}, Pt^{2+}, Cd^{2+}, Pb^{2+}, Cr^{3+}, Ba^{2+} and Pd^{2+}, were added at up to 5.0 equiv. to the solution of **YPT** (10 μM); as shown in

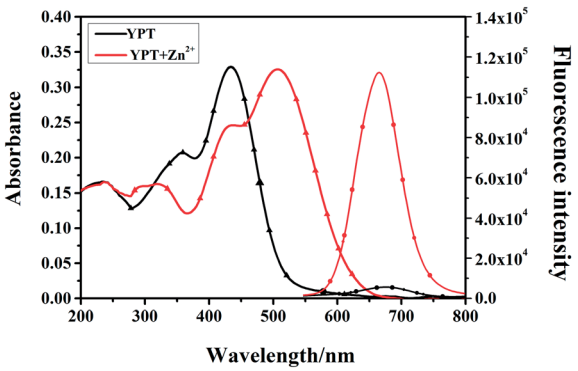

Fig. 1 The absorption (▲) and emission (●) spectra of YPT (black line) and YPT + Zn^{2+} (red line) in DMSO–H_2O (3 : 2 v/v, pH 7.4, HEPES buffer, 0.5 mM).

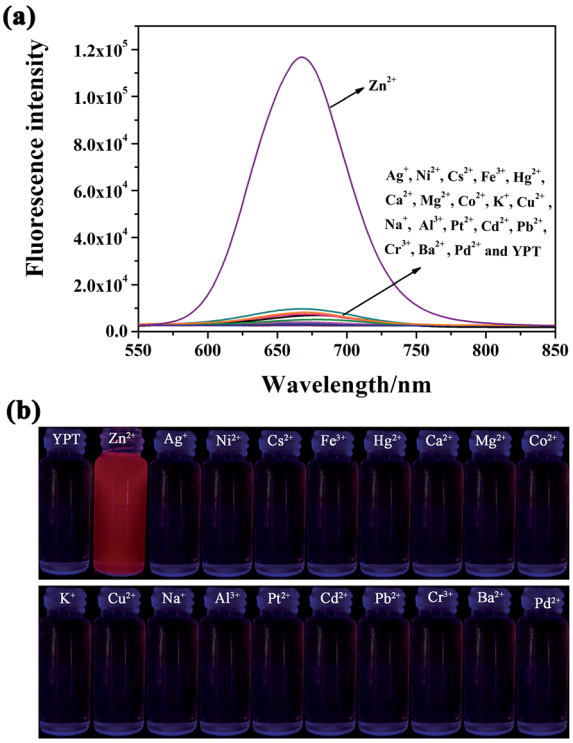

Fig. 2 (a) Fluorescence spectral changes of **YPT** (10 μM) in DMSO–H_2O (3 : 2 v/v, pH 7.4, HEPES buffer, 0.5 mM) after the addition of various metal ions at 5.0 equiv. (b) Color changes of **YPT** (10 μM) upon the addition of Zn^{2+} (5.0 equiv.) and other metal ions (5.0 equiv.) in DMSO–H_2O (3 : 2 v/v, pH 7.4, HEPES buffer, 0.5 mM) under 365 nm UV light.

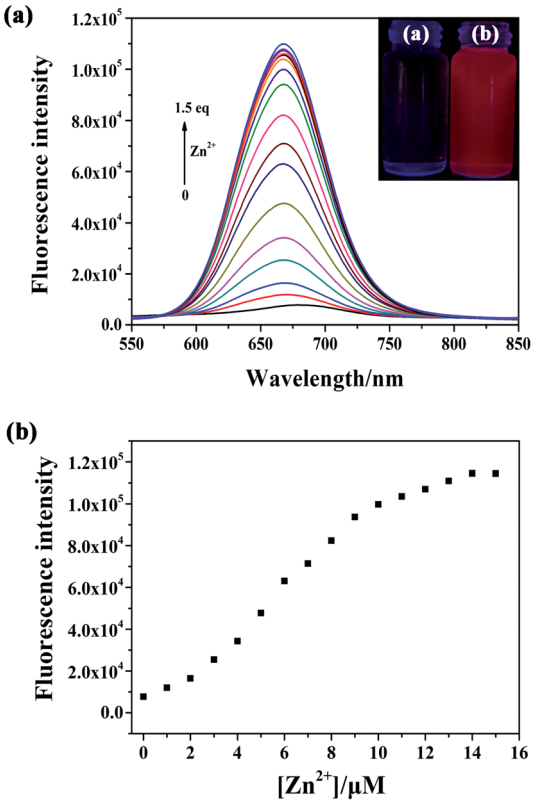

Fig. 3 (a) Fluorescence spectral changes of **YPT** (10 μM) upon the addition of different concentrations of Zn^{2+} (0.0–15 μM) in DMSO–H_2O (3 : 2 v/v, pH 7.4, HEPES buffer, 0.5 mM). Inset: fluorescence images of **YPT** (10 μM) in the absence (left) and presence (right) of Zn^{2+} under a 365 nm UV lamp. (b) A plot of fluorescence intensity changes at 670 nm of **YPT** (10 μM) as a function of Zn^{2+} concentrations.

Fig. 2a and b, only the addition of Zn^{2+} induced an obvious fluorescence enhancement at 670 nm, whereas the addition of other metals induced only negligible changes. This result indicates that **YPT** is highly selective for Zn^{2+} over other metals.

3.3 Sensitivity of YPT

To evaluate the sensitivity of **YPT**, the fluorescence titrations of **YPT** against Zn^{2+} in DMSO–H_2O (3 : 2 v/v, pH 7.4, HEPES buffer, 0.5 mM) were performed, and the titration data are depicted in Fig. 3. With an increase in the concentration of Zn^{2+} (0–1.5 equiv.) in the solution of **YPT** (10 μM), the fluorescence intensity of **YPT** increased gradually (maxima at 670 nm) with a 168 nm Stokes shift because of the complexation of **YPT** with Zn^{2+}. Moreover, we could observe that the probe solution had almost no fluorescence upon the addition of Zn^{2+} at different concentrations to the solution of **YPT**; however, a strong red fluorescence was observed under a 365 nm UV lamp (Fig. 3a). When 1.5 equiv. of Zn^{2+} was added, the fluorescence intensity gradually reached a maximum at 1.0 equiv. (Fig. 3b). Furthermore, a good relationship between the fluorescence intensity at 670 nm and the concentration of Zn^{2+} (1–10 μM) was obtained with $R^2 = 0.9906$ ($y = 1.0548 \times 10^4 \times -3.3884 \times 10^3$) (Fig. S17†).[45,46] The limit of detection was calculated to be 12 nM on the basis of $3\sigma/S$. Moreover, the association constant was calculated to be $8.33 \times 10^4\ M^{-1}$ using the Benesi–Hildebrand equation based on the result of fluorescence titrations (Fig. S18†).[47] These results indicated high sensitivity of **YPT** towards Zn^{2+}.

3.4 Job's plot of YPT and Zn^{2+}

Solutions of Zn^{2+} and **YPT** were prepared with a total concentration of 50 μM, and the mole fraction of Zn^{2+} to **YPT** ranged

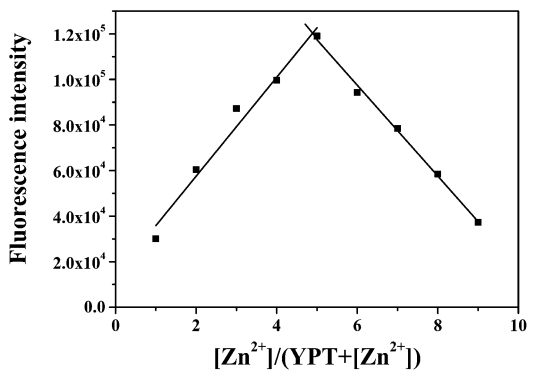

Fig. 4 Job's plot of **YPT** complexed with Zn^{2+} in DMSO–H_2O (3 : 2, pH 7.4, HEPES buffer, 0.5 mM).

from 0 to 1. As shown in Fig. 4, the Job's plot for the binding between **YPT** and Zn^{2+} revealed a 1 : 1 stoichiometry.

3.5 Effect of other competitive metal ions

A competitive experiment was conducted to estimate the specificity of **YPT** towards Zn^{2+} in DMSO–H_2O (3 : 2 v/v, pH 7.4, HEPES buffer, 0.5 mM). For the competition test, **YPT** was treated with 5.0 equiv. of Zn^{2+} in the presence of various competitive ions (5.0 equiv.), including Ag^{+}, Ni^{2+}, Cs^{2+}, Fe^{3+}, Hg^{2+}, Ca^{2+}, Mg^{2+}, Co^{2+}, K^{+}, Cu^{2+}, Na^{+}, Al^{3+}, Pt^{2+}, Cd^{2+}, Pb^{2+}, Cr^{3+}, Ba^{2+} and Pd^{2+}, in DMSO–H_2O (3 : 2 v/v, pH 7.4, HEPES buffer, 0.5 mM). As shown in Fig. 5, the fluorescence intensities of the **YPT**–Zn^{2+} solution did not show obvious interferences from the interfering metal ions.

Thus, the designed probe **YPT** could be used as an excellent probe with high selectivity for Zn^{2+} in the presence of various other metal ions.

3.6 Effect of pH on Zn^{2+} sensing

A suitable pH range is an essential factor for the detection of Zn^{2+} in environmental systems. The spectral response of the probe **YPT** was investigated in the pH range 2.0–12.0 in DMSO–H_2O (3 : 2 v/v, pH 7.4, HEPES buffer, 0.5 mM). As shown in Fig. S19,† **YPT** showed very low fluorescence intensity in pH 2.0–12.0. Upon the addition of Zn^{2+}, the fluorescence intensity at 670 nm rapidly increased obviously from 5.0 to 8.0. These results clearly indicate that **YPT** can be used as a probe to detect Zn^{2+} under physiological conditions.

3.7 Effect of response time on Zn^{2+} sensing

To obtain an appropriate reaction time, time-independent modulation in the fluorescence spectra was monitored in the presence of 5.0 equiv. of Zn^{2+}. As displayed in Fig. 6, it could be observed that the fluorescence intensity increased rapidly and reached a plateau in just 30 s. This result suggested that **YPT** could potentially serve as a detector for the real-time monitoring of Zn^{2+}.

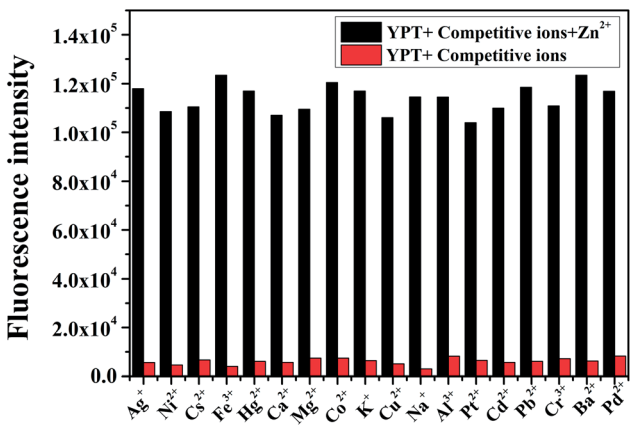

Fig. 5 Fluorescence intensity changes at 670 nm of **YPT** (10 μM) towards Zn^{2+} (5.0 equiv.) in the presence of other competitive metal ions (5.0 equiv.) in DMSO–H_2O (3 : 2 v/v, pH 7.4, HEPES buffer, 0.5 mM).

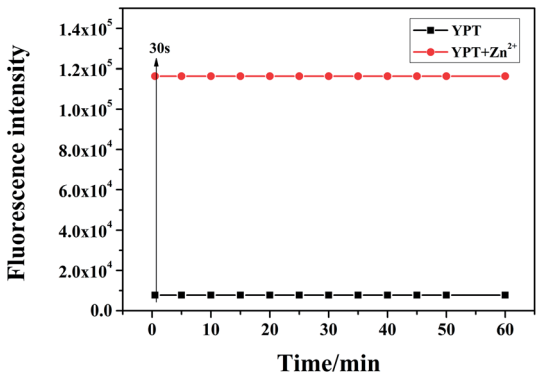

Fig. 6 Time-dependent intensity changes of only **YPT** (10 μM) and upon the addition of Zn^{2+} (5.0 equiv.) in DMSO–H_2O (3 : 2 v/v, pH 7.4, HEPES buffer, 0.5 mM).

3.8 The proposed sensing mechanism

ESI-mass spectrometry analysis. The peak at *m*/*z* 589.2471 obtained before complexation corresponded to $[\mathbf{YPT}–H]^{+}$ (Fig. S20†). Upon the addition of Zn^{2+} to the solution of **YPT**, the mass spectrometry peak appeared at *m*/*z* 653.1765 (Fig. S21†). This was assigned to the complex $[\mathbf{YPT}^{2-} + Zn^{2+} + H^{+}]^{+}$ and the 1 : 1 binding model between **YPT** and Zn^{2+}.

To better understand the binding site of **YPT** with Zn^{2+}, ^{1}H NMR titration experiments were carried out in DMSO-d_6. As shown in Fig. S22,† upon the addition of Zn^{2+} at 0–4 equiv. concentrations, the peaks of the phenolic –OH (a), the imine –NH (b) and –CH=N– (c) were gradually weakened. This result might confirm that **YPT** might chelate Zn^{2+} by the coordination of the oxygen atom of the phenolic –OH, the nitrogen atom of the imine –NH on purine and the nitrogen atom of –CH=N– with Zn^{2+}.

To further investigate the binding mechanism of **YPT** with Zn^{2+}, we performed DFT calculations using the B3LTP/6-31G* method. The spatial distributions and orbital energies of the HOMO and LUMO of the **YPT** and **YPT**–Zn^{2+} complex were investigated and are shown in Fig. 7. The HOMO–LUMO energy bands of **YPT** and **YPT**–Zn^{2+} were respectively calculated as 0.09043 a.u. and 0.0883.8 a.u., which exhibited that the binding of Zn^{2+} to **YPT** lowered the HOMO–LUMO energy gap of **YPT**. This result suggested that the chelation of Zn^{2+} with **YPT** stabilized the energy of PET transition. Based on the above-mentioned studies, the proposed mechanism for the recognition of Zn^{2+} by ZPT is shown in Scheme 2.

3.9 Fast detection of Zn^{2+} with the test strips

For practical application, we used test strips containing the probe **YPT** to detect Zn^{2+}. The filter papers were immersed in a solution of **YPT** (1 mM) and then dried in air. After the test strips were exposed to Zn^{2+} at different concentrations for several seconds and dried in air, we could observe that the test strips underwent a rapid colour change under 365 nm UV light.

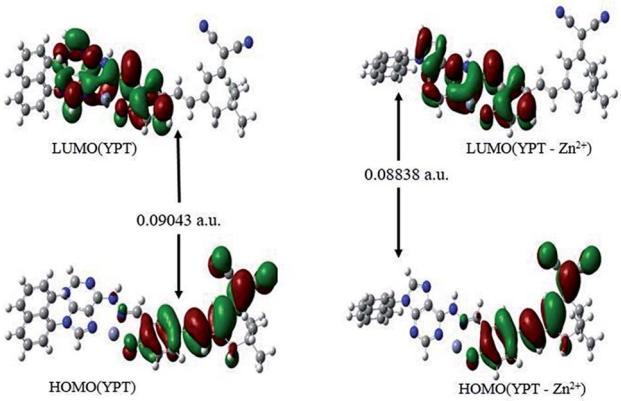

Fig. 7 HOMO and LUMO orbitals of the YPT and YPT–Zn^{2+} complexes.

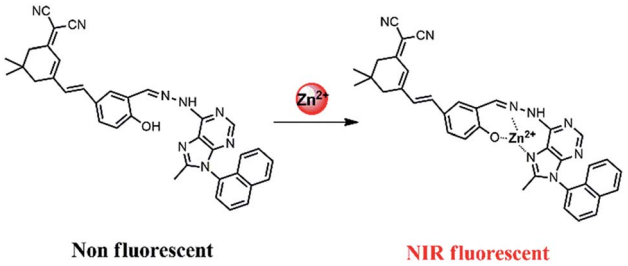

Scheme 2 Fluorescence enhancement mechanism of the YPT–Zn^{2+} complex.

As shown Fig. 8, the test strips displayed colorimetric changes from being colourless to red under 365 nm UV light. Thus, **YPT** can be used as a test paper for the quantitative detection of Zn^{2+} without any instrumental analysis.

3.10 Cell experiments

To examine the ability of **YPT** to track the level of intracellular Zn^{2+}, cytotoxicity investigation and fluorescence imaging experiments were carried out. The standard MTT assays for HeLa cells at different concentrations (0–20 μM) were performed to determine the cytotoxicity of **YPT**. The estimated cellular viability was over 80% after 24 h, indicating that the probe **YPT** had low cytotoxicity and could be used to detect Zn^{2+} in living cells (Fig. S23†). Next, fluorescence imaging experiments were carried out in HeLa cells, and a confocal laser microscope was used for fluorescence imaging. The HeLa cells were incubated with **YPT** (10 μM) for 30 min at 37 °C. As shown in Fig. 9a, the probe **YPT** in the cell nucleus showed no fluorescence signal. As shown in Fig. 9b, it displayed strong bright fluorescence after incubation with Zn^{2+}. These results indicate that the probe **YPT** can be used for the fluorescence imaging of Zn^{2+} in living cells.

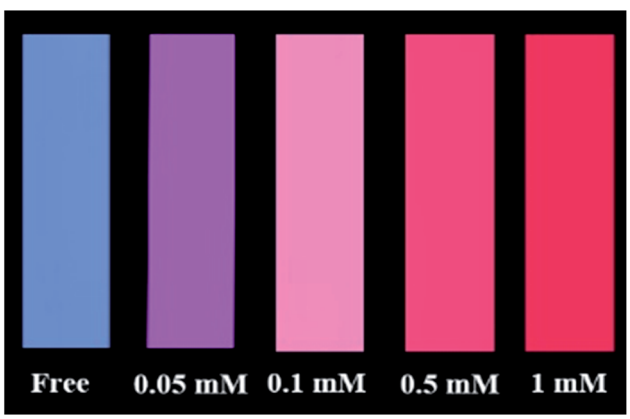

Fig. 8 Images of the test strips of YPT treated with of Zn^{2+} at different concentrations under 365 nm UV light.

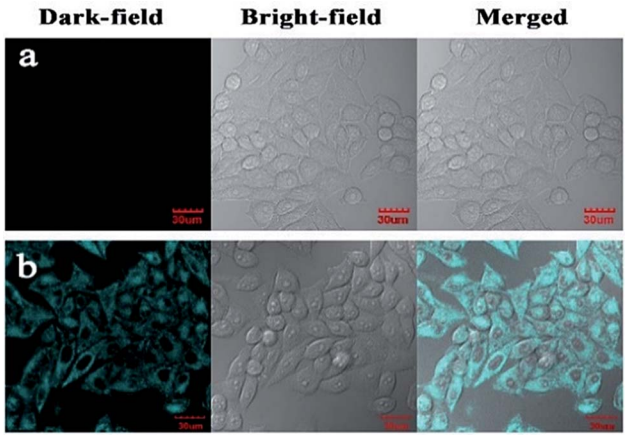

Fig. 9 Fluorescence imaging of YPT (10 μM) in HeLa cells in the (a) absence and (b) presence of Zn^{2+} (20 μM).

4. Conclusions

In summary, we synthesized a novel "off–on" fluorescent probe **YPT** based on a dicyanoisophorone derivative for the detection of Zn^{2+}. **YPT** displayed extremely high selectivity and sensitivity for Zn^{2+} in DMSO–H_2O (3 : 2 v/v, pH 7.4, HEPES buffer, 0.5 mM). In addition, the probe **YPT** showed a rapid response time (30 s), a good binding constant (8.33×10^4 M^{-1}) and a low detection limit (12 nM). Moreover, Job's plot, HR-MS, ^1H NMR titration analysis and DFT calculations showed the response mechanism of **YPT** towards Zn^{2+}. The cell experiments demonstrated that the probe could be used to detect intracellular Zn^{2+} in living cells. Furthermore, the probe **YPT** could be made into test papers to detect Zn^{2+} by naked eyes.

Conflicts of interest

There are no conflicts to declare.

Acknowledgements

This work was supported by the Qing Lan Project of Jiangsu Province and Postgraduate Research & Practice Innovation Program of Jiangsu Province.

Notes and references

1 M. Wolfgang and L. Yuan, Coordination Dynamic of Zinc in Proteins, *Chem. Rev.*, 2009, **109**, 4782.

2 B. L. Vallee and K. H. Falchuk, The Biochemical Basis of Zinc Physiology, *Physiol. Rev.*, 1993, **73**, 79.

3 Z. Xu, G.-H. Kim, S. J. Han, M. J. Jou, C. Lee, I. Shin and J. Yoon, An NBD-based colorimetric and fluorescent chemosensor for Zn^{2+} and its use for detection of intracellular zinc ions, *Tetrahedron*, 2009, **65**, 2307.

4 J. F. Zhang, S. Bhuniya, Y. H. Lee, C. Bae, J. H. Lee and J. S. Kim, Novel 2,2′-bipyridine-modified calix[4]arenes: ratiometric fluorescent chemosensors for Zn^{2+} ion, *Tetrahedron Lett.*, 2010, **51**, 3719.

5 Y. Qian, C. Wang and F. Gao, Ultrasensitive electrochemical detection of DNA based on Zn^{2+} assistant DNA recycling followed with hybridization chain reaction dual amplification, *Biosens. Bioelectron.*, 2015, **63**, 425.

6 Y. Qian, C. Wang and F. Gao, Assistant deoxyribonucleic acid recycling with Zn^{2+} beacon for electrochemical detection of deoxyribonucleic acid *via* target-triggered assembly of mutated DNAzy/me, *Anal. Chim. Acta*, 2014, **845**, 1.

7 C. J. Frederickson, Neurobiology of zinc and ainc-containing neurons, *Int. Rev. Neurobiol.*, 1989, **31**, 145.

8 J. H. Kim, I. H. Hwang, S. P. Jang, J. Kang, S. Kim, I. Noh, Y. Kim, C. Kim and R. G. Harrison, Zinc sensors with lower binding affinities for cellular imaging, *Dalton Trans.*, 2013, **42**, 5500.

9 A. I. Bush, The metallobiology of Alzheimer's disease, *Trends Neurosci.*, 2003, **26**, 207.

10 G. J. Park, H. Kim, J. J. Lee, Y. S. Kim, S. Y. Lee, S. Lee, I. Noh and C. Kim, A highly selective turn-on chemosensor capable of monitoring Zn^{2+} concentrations in living cells and aqueous solution, *Sens. Actuators, B*, 2015, **215**, 568.

11 V. Bhalla, Roopa and M. Kumar, Pentaquinone based probe for nanomolar detection zinc ions: Chemosensing ensemble as an antioxidant, *Dalton Trans.*, 2013, **42**, 975.

12 P. Pohl, Determination of metal content in honey by atomic absorption and emission spectrometries, *TrAC, Trends Anal. Chem.*, 2009, **28**, 117.

13 J. Chen and K. C. Teo, Determination of cadmium, copper, lead and zinc in water samples by flame atomic absorption spectrometry after cloud point extraction, *Anal. Chim. Acta*, 2001, **450**, 215.

14 J. S. Becker, A. Matusch, C. Depboylu, J. Dobrowolska and M. V. Zoriy, Quantitative Imaging of Selenium, Copper, and Zinc in Thin Sections of Biological Tissues (Slugs-Genus Arion) Measured by Laser Ablation Inductively Coupled Plasma Mass Spectrometry, *Anal. Chem.*, 2007, **79**, 6074.

15 E. L. Silva, S. Roldan Pdos and M. F. Gine, Simultaneous preconcentration of copper, zinc, cadmium, and nicker in water samples by cloud point extraction using 4-(2-pyridylazo)-resorcinol and their determination by inductively coupled plasma optic emission spectrometry, *J. Hazard. Mater.*, 2009, **171**, 113.

16 P. R. d. Oliveira, A. C. Lamy-Mendes, J. L. Gogola, A. S. Mangrich, L. H. Marcolino Junior and M. F. Bergamini, Mercury nanodroplets supported at biochar for electrochemical determination of zinc ions using a carbon paste electrode, *Electrochim. Acta*, 2015, **151**, 525.

17 L. E. Mcquade and S. J. Lippard, Cell-Trappable Quinoline-Derivatized Fluoresceins for Selective and Reversible Biological Zn(II) Detection, *Inorg. Chem.*, 2010, **49**, 9535.

18 Z. Xu, J. Yoon and D. R. Spring, Fluorescent chemosensors for Zn^{2+}, *Chem. Soc. Rev.*, 2010, **39**, 1996.

19 J. Yan, L. Fan, J. Qin, C. Li and Z. Yang, A novel and resumable Schiff-base fluorescent chemosensor for Zn(II), *Tetrahedron Lett.*, 2016, **57**, 2910.

20 J. An, M. Yan, Z. Yang, T. Li and Q. Zhou, A turn-on fluorescent sensor for Zn(II) based on fluorescein-coumarin conjugate, *Dyes Pigm.*, 2013, **99**, 1.

21 J. Nie, N. Li, Z. Ni, Y. Zhao and L. Zhang, A sensitive tetraphenylethene-based fluorescent probe for Zn^{2+} ion involving ESIPT and CHEF process, *Tetrahedron Lett.*, 2017, **58**, 1980.

22 M. Yang, Y. Zhang, W. Zhu, H. Wang, J. Huang, L. Cheng, H. Zhou, J. Wu and Y. Tian, Difunctional chemosensor for Cu(II) and Zn(II) based on Schiff base modified anthryl derivative with aggregation-induced emission enhancement and piezochromic characteristics, *J. Mater. Chem. C*, 2015, **3**, 1994.

23 I. Roy, J.-Y. Shin, D. Shetty, J. K. Khedkar, J. H. Park and K. Kim, E-BODIPY fluorescent chemosensor for Zn^{2+} ion, *J. Photochem. Photobiol., A*, 2016, **331**, 233.

24 S. L. Zhu, J. T. Zhang, J. Janjanam, G. Vegesna, F. T. Lou, A. Tiwari and H. Y. Liu, Highly water-soluble BODIPY-based fluorescent probes for sensitive fluorescent sensing of zinc(II), *J. Mater. Chem. B*, 2013, **1**, 1722.

25 Y. Gao, H. Liu, P. Li, Q. Liu, W. Wang and B. Zhao, Coumarin-based fluorescent chemosensor for the selective quantification of Zn^{2+} and AcO^{-} in an aqueous solution and living cells, *Tetrahedron Lett.*, 2017, **58**, 2193.

26 N. Zhang, X. Tian, J. Zheng, X. Zhang, W. Zhu, Y. Tian, Q. Zhu and H. Zhou, A novel fluorescent probe based on the flexible dipicolylamine: Recognizing zinc(II) in aqueous solution and imaging in living cell, *Dyes Pigm.*, 2016, **124**, 174.

27 Y. Xia, H. Zhang, X. Zhu, Q. Zhang, M. Fang, X. Li, H. Zhou, X. Yang, X. Zhang and Y. Tian, Two-photo fluorescent probe with enhanced absorption cross section for relay recognition of $Zn^{2+}/P_2O_7^{4-}$ and *in vivo* imaging, *Spectrochim. Acta, Part A*, 2018, **204**, 446.

28 W. Li, X. Tian and B. Huang, Triphenylamine-based Schiff bases as the High sensitive Al^{3+} or Zn^{2+} fluorescence turn-on probe: Mechanism and application *in vitro* and *in vivo*, *Biosens. Bioelectron.*, 2016, **77**, 530.

29 S. A. Yoon, J. Lee and M. H. Lee, A ratiometric fluorescent probe for Zn^{2+} based on pyrene-appended naphthalimide–dipicolylamine, *Sens. Actuators, B*, 2018, **258**, 50.

30 Y. Tang, Y. Huang, L. Lu, C. Wang, T. Sun, J. Zhu, G. Zhu, J. Pan, Y. Jin, A. Liu and M. Wang, Synthesis of a new

pyrene-derivative fluorescent probe for the detection of Zn^{2+}, *Tetrahedron Lett.*, 2018, **59**, 3916.

31 D. Wu, L. Chen, W. Lee, G. Ko, J. Yin and J. Yoon, Recent progress in the development of organic dyes based near-infrared fluorescence probes for metal ions, *Coord. Chem. Rev.*, 2018, **354**, 74.

32 K. Kiyose, H. Kojima and T. Nagano, Functional Near-Infrared Fluorescent Probes, *Chem.–Asian J.*, 2008, **3**, 506.

33 L. Yuan, W. Lin, K. Zheng, L. He and W. Huang, Far-red to near infrared analyte-responsive fluorescent probes based on organic fluorophore platforms for fluorescence imaging, *Chem. Soc. Rev.*, 2013, **42**, 622.

34 Z. Guo, S. Park, J. Yoon and I. Shin, Recent progress in the development of near-infrared fluorescent probes for bioimaging applications, *Chem. Soc. Rev.*, 2014, **43**, 16.

35 D. Yu, F. Huang, S. Ding and G. Feng, Near-Infrared Fluorescent Probe for Detection of Thiophenols in Water Samples and Living Cells, *Anal. Chem.*, 2014, **86**, 8835.

36 S. Xue, S. Ding, Q. Zhai, H. Zhang and G. Feng, A readily available colorimetric and near-infrared fluorescent turn-on probe for rapid and selective detection of cysteine in living cells, *Biosens. Bioelectron.*, 2015, **68**, 316.

37 M. Li, W. Feng, Q. Zhai and G. Feng, Selenocysteine detection and bioimaging in living cells by a colorimetric and near-infrared fluorescent turn-on probe with a large stokes shift, *Biosens. Bioelectron.*, 2017, **87**, 894.

38 J. Hong, W. Feng and G. Feng, Highly selective near-infrared fluorescent probe with rapid response, remarkable large Stokes shift and bright fluorescence for H_2S detection in living cells and animals, *Sens. Actuators, B*, 2018, **262**, 837.

39 J. Hong, E. Zhou, S. Gong and G. Feng, A red to near-infrared fluorescent probe featuring a super large Stokes shift for light-up detection of endogenous H_2S, *Dyes Pigm.*, 2019, **160**, 787.

40 O. Kwon, S. Kwon, M. Jazbinsek, F. D. J. Brunner, J.-I. Seo, C. Hunziker, A. Schneider, H. Yun, Y.-S. Lee and P. Günter, Organic Phenolic Configurationally Locked Polyene Single Crystal for Electro-optic and Teraherta Wave Applications, *Adv. Funct. Mater.*, 2008, **18**, 3242.

41 Z. Guo, W. Zhu and H. Tian, Dicyanomethylene-4*H*-pyran chromophores for OLED emitters, logic gates and optical chemosensors, *Chem. Commun.*, 2012, **48**, 6073.

42 H. Lu, L. Zhang, D. Wu and J. Zhou, Microwave Assisted Synthesis of 2,6-Substituted Aromatic Aminopurine Derivatives, *J. Heterocycl. Chem.*, 2011, **48**, 1140.

43 X. Jin, H. Chen, W. Zhang, B. Wang, W. Shen and H. Lu, A novel purine derivative-based colorimetric chemosensor for sequential detection of copper ion and sulfide anion, *Appl. Organomet. Chem.*, 2018, **32**, 1.

44 G. Wu, Z. Wang, W. Zhang, W. Chen, X. Jin and H. Lu, A novel rhodamine B and purine derivative-based fluorescent chemosensor for detection of palladium(II) ion, *Inorg. Chem. Commun.*, 2019, **102**, 233.

45 H. A. Benesi and J. H. Hildebrand, A Spectrophotometric Investigation of Interaction of Iodine with Aromatic Hydrocarbons, *Chem. Rev.*, 1949, **71**, 2703.

46 H. Chen, X. Jin, W. Zhang, H. Lu and W. Shen, A new rhodamine B-based 'off–on' colorimetric chemosensor for Pd^{2+} and its imaging in living cells, *Inorg. Chim. Acta*, 2018, **482**, 122.

47 Y. Shiraishi, S. Sumiya and T. Hirai, Highly sensitive cyanide anion detection with a coumarin-spiropyran conjugate as a fluorescent receptor, *Chem. Commun.*, 2011, **47**, 4953.